Engineering Structures 195 (2019) 425–437

Contents lists available at ScienceDirect

Engineering Structures

journal homepage: www.elsevier.com/locate/engstruct

Uncertainty quantification of fragility and risk estimates due to seismic input variability and capacity model uncertainty

Despoina Skoulidou*, Xavier Romão

CONSTRUCT-LESE, Faculty of Engineering, University of Porto, Rua Dr. Roberto Frias, 4200-465 Porto, Portugal

ARTICLE INFO

Keywords:
Fragility function
Parameter variability
Failure rate variability
Probabilistic capacity
Bootstrap

ABSTRACT

When evaluating the probabilistic seismic performance of a structure in the context of Performance-Based Earthquake Engineering (PBEE) applications, only estimates of the true response are obtained due to the finite size of the group of records selected to represent the seismic scenario. The proposed study examines the variability of these estimates, in terms of fragility parameters and failure rates, by implementing a procedure that creates seismic scenario-consistent groups of records based on regrouping criteria applied to a larger set of records. The results are then compared to those obtained from a statistical approach based on the bootstrap resampling procedure, whose validity is disputed due to its incompatibility with common applications involving probabilistic seismic performance assessment. Given that bootstrap resampling assumes that each bootstrap sample is random, this condition is incompatible with requirements involving the need to match specific spectral statistics of the group of records with a target spectrum. Due to the increased computational cost of the procedure based on regrouping criteria, the effect of this incompatibility is analysed by examining the agreement between the two procedures for several case studies and the conditions under which bootstrap resampling leads to a reduced level of error. Further insights about the variability of the estimates are obtained by analysing scenarios with deterministic and probabilistic thresholds of the limit state capacity. Among other aspects, the results show that, for both capacity thresholds, bootstrap resampling can provide acceptable results as long as a sufficient number of ground motions and number of stripes are used.

1. Introduction

Practical guidelines provided by the Performance-Based Earthquake Engineering framework for the probabilistic assessment of the seismic performance of a building [1] draw attention to various sources of uncertainty. Common sources are those associated with the seismic input, usually expressed by the seismic hazard uncertainty [2] and the record-to-record variability [3], the structural modelling, such as the variability of geometric properties and material constitutive laws [1], and limit state definitions, like the capacity modelling errors [4]. These uncertainties can be accounted for during the structural analysis of the numerical model or in a subsequent post-processing stage of the analysis results. Depending on the stage of the analysis in which the different uncertainties are accounted for, their combination can be performed using Monte Carlo simulation-based techniques or alternative simplified methods, such as first-order second-moment techniques (e.g. see [5–9]). Nevertheless, it is commonly agreed that accounting for uncertainties changes the seismic demand, the fragility function parameters [10], the associated seismic risk [11,12], as well as the expected losses [13].

The present research analyses the variability of the fragility function parameter estimates and of the associated seismic risk estimates due to uncertainty of the input seismic action when nonlinear dynamic analysis is performed. In nonlinear dynamic analysis, the size of the considered group of ground motion records is selected in order to capture record-to-record variability and, at the same time, to accommodate availability and computational time-related restrictions. However, due to the finite size of the group of records, only an estimate of the seismic demand is obtained and it can be argued that a different group of records, representative of the same seismic scenario, would lead to a different estimate of the same demand [14]. Existing procedures commonly used to account for the uncertainty associated to the use of a finite size group of records, termed group-to-group[1] variability hereon, rely on analytical procedures, such as the Delta method, or on

* Corresponding author.
E-mail address: dskoulidou@fe.up.pt (D. Skoulidou).

[1] The term group-to-group variability is used herein to differentiate from the record-to-record variability, which refers to the variability of the seismic input due to the different properties of the records within the same group.

https://doi.org/10.1016/j.engstruct.2019.05.067
Received 30 August 2018; Received in revised form 14 March 2019; Accepted 22 May 2019

numerical simulations, such as the *bootstrap resampling*, [12,14,15]. The applicability of each procedure depends on the methodology applied to derive the fragility functions, the desired precision as well as time- and computation-related restrictions. Given its widespread use (e.g. see [16–19]), as well as the possibility to combine multiple sources of epistemic uncertainty [15], the *bootstrap resampling* is found to be the most commonly used procedure to assess group-to-group variability.

One of the main conditions of *bootstrap resampling* is that *bootstrap* samples are random samples [20]. However, this condition is not always compatible with a situation involving the resampling of groups of records (each group of records being a sample) where the properties of each group need to match those of a certain seismic scenario. Enforcing a match between statistics representative of the sample (i.e. the group of records) and parameters of the selected seismic scenario conditions the sample, since it is by combining those specific records that the sample is valid (where valid means that it matches the parameters of the seismic scenario). Therefore, by conditioning the way it is defined, a sample cannot be considered to be random. To take this issue into account, an alternative procedure is proposed that involves creating new groups of records based on a process that regroups selected earthquake records and maintains the compatibility with the seismic scenario for all new groups.

The variability of the estimates of the fragility function parameters and of the associated seismic risk is determined according to the proposed procedure, i.e. the *regrouping* procedure, and is then compared to the variability obtained using the *bootstrap resampling* procedure. Even though *bootstrap resampling* is inconsistent (see Section 3.1 for a more detailed discussion), since the *regrouping* procedure is more computationally demanding, the ability of *bootstrap resampling* to provide variability estimates that are adequate is analysed by comparing them to those obtained by the *regrouping* procedure. The comparisons are performed using structural response data obtained from the nonlinear dynamic analysis of three structures for increasing levels of earthquake loading. Furthermore, fragility parameter estimates and risk estimates are analysed for two scenarios of the limit state capacity: one that considers deterministic capacity and one that considers probabilistic capacity, the latter leading to counterintuitive observations regarding the variability of the estimates.

2. Modelling the fragility function and the rate of failure

The probability of failure $P(f)$ of the structure given the seismic intensity measure (*IM*), also termed the fragility function, is often conveniently represented by a lognormal cumulative distribution function (CDF):

$$P[f|IM = im] = \Phi\left(\frac{\log(im/\theta)}{\beta}\right) \tag{1}$$

where Φ is the standard normal CDF with parameters $\log(\theta)$ and β. Fragility functions are usually derived based on numerical analysis results obtained from an inelastic structural model subjected to a group of hazard-consistent records applied with various intensities. Currently available methodologies for deriving numerical simulation-based fragility functions can be grouped into IM-based and EDP-based methodologies, according to [21]. A compilation of fragility curve generation procedures based on nonlinear analysis can also be found in [22], including additional information about other features such as the consideration of non-deterministic capacity limit states. For the purpose of the present study, an EDP-based approach [21] will be applied, using analytically compatible numerical analysis results from multiple-stripe analyses (MSA) [23]. Briefly, MSA involves groups of records, each selected to be hazard-compatible at a specific *IM* level (i.e. each stripe level), applied to the structure whose response, conditional to the predefined intensity, is defined by Engineering Demand Parameters (EDPs). The generated group of EDPs is also termed a stripe of EDPs and multiple intensity levels are considered to generate multiple stripes of EDPs. The EDPs of each stripe are compared to their corresponding capacities and, for each comparison, a failure/no failure state of the structure is assigned. The term failure is considered herein as reflecting the inability of the structure to comply with predetermined criteria and can be associated to any predefined limit state or performance measure. Furthermore, for the purpose of the current study, each limit state is conditioned by one EDP. To derive the function of Eq. (1) according to the EDP-based approach, the total number of analyses at each *IM* level z_{IM} is partitioned into the number of analyses that led to failure of the structure c_{IM} and the complementary number of analyses that didn't cause failure. Subsequently, the ratios:

$$p_{IM} = \frac{c_{IM}}{z_{IM}} \tag{2}$$

are determined for each *IM* level, indicating the probability of failure of the structure at a given *IM* level. By considering all failure and no failure observations to be independent, the binomial distribution can be used to express the probability of having c_{IM} failures in z_{IM} records at each *IM* level and the fragility function parameters of Eq. (1) can then be determined using the maximum likelihood estimation procedure suggested in [21].

The fragility function can then be numerically integrated with the derivative of the seismic hazard curve dH_{IM} to yield the mean failure rate of the structure (simply termed failure rate hereon):

$$\lambda_f = \int_0^\infty P[f|IM]\,|dH_{IM}| \tag{3}$$

Finally, assuming that both hazard and fragility are memoryless, failure can be considered to be a Poisson process and the probability of failure, i.e. the risk of failure, can be derived by:

$$P_f = 1 - e^{-\lambda_f} \tag{4}$$

which, in case of small failure rates, can be considered equal to the failure rate without significant error.

3. Methodology to analyse the performance of the procedures assessing the variability of fragility and failure rate estimates

The following sections describe the different type of scenarios and methodological approaches considered in the case studies of Section 4 to compare the performance of the *regrouping* and *bootstrap resampling* procedures in assessing the variability of fragility parameter estimates and failure rate estimates.

3.1. Analysing the variability of fragility parameter estimates due to group-to-group variability

The fragility function parameters determined using a particular group of records are estimates $\{\hat{\theta}, \hat{\beta}\}$ of the true unknown parameters $\{\theta, \beta\}$ due to the relatively small (finite) number of records used to represent the seismic input [12,14]. It is therefore expected that a different group of records will lead to a different set of $\{\hat{\theta}, \hat{\beta}\}$. The variability of the fragility parameters obtained from the EDP-based approach due to group-to-group variability can thus be determined using a large number of groups of records obtained using the same selection criteria. A procedure simulating this rationale is applied herein, according to which a number N of records is initially selected and used to perform MSA of the structural model. Next, multiple groups of records with a smaller size n (with $n < N$) are created by regrouping n records of the initial N and enforcing the same selection criteria. This procedure, termed the *regrouping* procedure hereafter, aims to create m new groups of n records consistent with the original seismic scenario. The EDPs corresponding to each new group are then post-processed according to Section 2 and m fragility functions are created, allowing for the statistical analysis of their variability.

As an alternative to using a large number of groups, i.e. the *regrouping* procedure described before, *bootstrap resampling* is often applied to examine the effect of the group-to-group variability on the fragility parameters, as described in [12]. This procedure, referred to as the *bootstrap* procedure hereon, considers a group of records of size n (i.e. the parent group) associated to a certain *IM* level and resamples it by selecting n records with replacement from this group (some of the records will appear more than once and others will not be present in the resampled group). The n failure/no-failure observations that correspond to the demand associated to this resampled group of records represents a demand pseudo-sample of size n for the selected *IM* level. Repeating this resampling procedure for all the *IM* levels (using the same parent group) generates the demand pseudo-samples needed to obtain the ratios defined by Eq. (2) for all *IM* levels and determine a new fragility function following the procedure described in Section 2. This procedure is then repeated m times (using the same parent group) to obtain m new fragility functions.

The *bootstrap* procedure generates consistent results as long as the two following assumptions are met: the data sample that is resampled (i.e. the parent sample) is representative of the population and is a random sample of the population. Under these conditions, the *bootstrap* procedure assumes that randomly resampling from the parent sample is equivalent to sampling from the population and that each *bootstrap* sample is a possible sample of the population [20]. In the context of the present study, where the parent sample is a group of ground motion records that need to fulfil a set of earthquake scenario compatibility criteria (see the spectral matching criteria defined in Section 4.2), the parent sample cannot be considered to have been randomly sampled from the population. By enforcing the referred earthquake scenario compatibility criteria, the parent sample is a conditioned sample, where conditioned means that certain criteria need to be met for the sample to be accepted as valid (see [24] for details on the optimization procedure that leads to the conditioned sample of records). Therefore, each resampled group of records randomly generated by bootstrapping the parent group of records are unlikely to fulfil the earthquake scenario compatibility criteria that led to the selection of the parent group. A simple example of this situation is the case where a group of n records is selected in order to have average spectral values over a certain period range that are within a ± 10% bound with respect to a certain target response spectrum. In this case, it can be understood that many random *bootstrap* combinations of those n records may not comply with the referred ± 10% bound. As other selection criteria are added to tighten the compatibility between the group of records and the target earthquake scenario (see Section 4.2 and the discussion in [24]), it is expected that most, if not all, of the bootstrap samples will not comply with the earthquake scenario compatibility criteria that are enforced.

In light of this, the value of the group-to-group variability obtained from the pseudo-samples generated by the *bootstrap* procedure is expected to be inconsistent with the value that would be obtained using a large number of groups, all selected to match the same earthquake scenario compatibility criteria, or using the *regrouping* procedure, that also enforces the same selection criteria. In order to analyse the significance of this inconsistency, the *regrouping* and the *bootstrap* procedures are applied to three case studies that also involve different numbers of group sizes and *IM* levels. Furthermore, since the *regrouping* procedure is more computationally demanding, the ability to still obtain adequate variability estimates with *bootstrap* is also analysed. Therefore, the performance of the procedures in determining the variability of fragility function parameter estimates and failure rate estimates is compared and the variability is quantified using statistics of the estimates (i.e. mean, standard deviation and coefficient of variation).

3.2. Analysing the variability of fragility parameter estimates due to group-to-group variability and uncertainty of the limit state capacity

The sets of fragility parameter estimates and associated statistics obtained according to Section 3.1 are determined by considering that the EDPs selected to establish the failure conditions have deterministic capacities (Cap_{det}). Additional sets of fragility parameter estimates and of the corresponding statistics were also determined by considering uncertainty in the capacity model of the EDPs. Existing research has shown the non-negligible influence of that source of uncertainty on both parameters of the lognormal fragility function, i.e. the shape and scale, [11,25]. The considered probabilistic capacity model (Cap_{prob}) is defined according to the following format:

$$Cap_{\text{prob}} = m_{Cap} \cdot \varepsilon_{Cap} \tag{5}$$

where m_{Cap} is the median value of the capacity model given as a function of deterministic geometry and material properties and ε_{Cap} is the error term accounting for scatter and bias of the capacity model. In the following, ε_{Cap} is assumed to be a lognormal random variable [26] with unit median, i.e. no bias, and dispersion β_{ε}. Variability in capacity is combined first with record-to-record variability and then with group-to-group variability as follows: for each record/analysis of a given group, the obtained EDPs are compared with a sample of k_{cap} equiprobable capacity values determined by Eq. (5) to define a series of failure/no-failure observations of size k_{cap}. The EDP-based procedure described in Section 2 is then applied, leading to one fragility function for each group of records (the algorithm that is used can be found in [22]). These new fragility parameter estimates involve uncertainty due to both the record-to-record variability and the uncertain capacity threshold. Finally, group-to-group variability is determined by applying both the *regrouping* and the *bootstrap* procedures as defined in Section 3.1 (i.e. by repeating this process for the n groups in the former, and by bootstrapping the sample of failure/no-failure observations of size $n \times k_{cap}$ in the latter). The performance of the two procedures is then compared as defined in Section 3.1, and the variability statistics are further compared with those obtained when considering a deterministic limit state capacity.

3.3. Analysing the variability of failure rate estimates

When a fragility function with parameter estimates $\{\hat{\theta}, \hat{\beta}\}$ is integrated with the seismic hazard according to Eq. (3), an estimate $\hat{\lambda}_f$ of the true unknown failure rate λ_f is obtained [12]. The variability associated to $\hat{\lambda}_f$ stems from the variability of the fragility function described in Sections 3.1 and 3.2, which is related to group-to-group variability and to how limit state capacity is defined (i.e. if it is deterministic or probabilistic), but it is also influenced by the seismic hazard curve, namely by the part of the curve contributing the most to the failure rate. By considering the multiple sets of fragility functions created in Sections 3.1 and 3.2, the corresponding sets of $\hat{\lambda}_f$ estimates are then obtained using Eq. (3). The variability of $\hat{\lambda}_f$ is then quantified for the several cases analysing statistics similar to those considered for the results of Sections 3.1 and 3.2.

4. Description of the selected case studies

4.1. Structural modelling

The selected case studies are three reinforced concrete buildings with infilled frame systems and with three, four and five storeys. All buildings have the plan view and the reinforcement detailing presented in Fig. 1. The structures are regular in-plan and in-elevation with a storey height equal to 3.0 m. The concrete strength and the yield strength of the reinforcement are equal to 25 MPa and 500 MPa, respectively. The buildings are located in Lisbon, Portugal and were

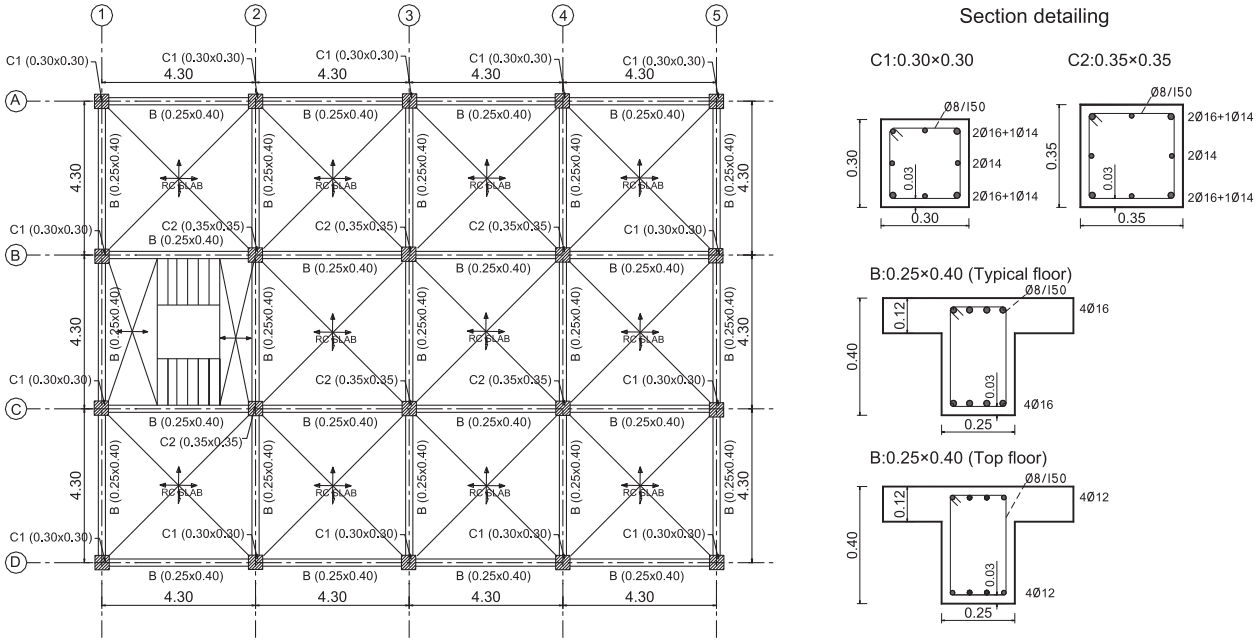

Fig. 1. Plan view of a typical storey of the three buildings and design details of the end sections of the elements (all dimensions are in m).

designed for gravity loads only. Specifically, a permanent load of 4 kN/m^2 is considered to be uniformly distributed on all floors, additional to the slab self-weight (all slabs have a 0.12 m thickness). Additionally, the quasi-permanent component of a uniform live load of 3 kN/m^2 is also assigned to all floors, except to the top floor where this load is 1 kN/m^2. Staircases are modelled only as permanent and quasi-permanent loads, which are transferred to the supporting beams and are applied uniformly. The corresponding loads are 7.75 kN/m and 8.60 kN/m for the permanent and the quasi-permanent loads, respectively. Masonry infills are present in all peripheral frames and represent a permanent uniform load of 7 kN/m.

Three-dimensional models of the buildings are simulated in the OpenSees (OS) computer software [27] considering mean values of all material and geometrical properties. A lumped plasticity approach is adopted to simulate the inelastic behaviour of all structural elements. Phenomenological hysteresis laws are assigned in rotational springs located on both ends of all columns and beams to simulate inelastic flexural behaviour. Two independent springs are assigned to each end of the columns, one for each orthogonal direction, while one spring is assigned to each end of the beams modelling the in-plane flexural behaviour. Due to the nature of the selected modelling approach, biaxial moment interaction or axial force moment interaction are not considered when modelling the behaviour of columns. The hysteretic flexural behaviour is defined by a moment-rotation law that is simulated using the *hysteretic* material provided by OS. The properties of the backbone curve of all columns are determined considering the axial force due to vertical loads of the seismic combination (G + 0.3Q), where G and Q stand for all permanent and quasi-permanent loads, respectively. The yielding moment (M_y) and the yielding rotation capacity (θ_y) are determined according to [28]. The capping (θ_c) and the ultimate (θ_u) rotation capacities are computed according to [29] along with the corresponding capping (M_c) and residual (M_r) moments, where the latter is considered to be 20% of M_c (see the backbone curve in Fig. 2(a)). Stiffness, strength and unloading stiffness degradation are considered in the hysteresis curves as shown in Fig. 2. The unloading stiffness degradation is implemented in OS via the beta factor of the *hysteretic* material. A beta factor of 0.75 is used for the columns and of 0.85 for the beams in order to introduce higher degradation for the latter [30]. The *hysteretic* material parameters related to pinching and to damage due to ductility and dissipated energy are all set equal to zero. The springs are connected in-series with a linear elastic interior element. A stiffness modification factor equal to 10 is applied according to [31] to account for the effect of the series connection on the total stiffness of the element. Beam-column node failure is not considered and rigid nodes are modelled in all element cross-sections. Even though the possibility of shear failure due to the weak detailing of the columns in flexure can be accounted for when post-processing the results of the analyses, the cases that are examined herein only deal with ductile demand which is defined by the maximum interstorey drift ratio of the two directions (ISD_{max}).

Masonry infills are considered in all peripheral frames and are modelled with a single strut active only in compression. Two diagonal struts (strut 1 and strut 2 as shown in Fig. 2 (b)) are used to simulate one infill and are connected to the beam-column joints. The equivalent area of each strut is established based on the maximum lateral force of the infill [32], transformed to the direction of the diagonal, and on the masonry compressive stress f_m. Maximum strength is assumed to be reached at an interstorey drift of 0.2% [33]. The lateral displacement of each infill is transformed into the diagonal displacement for the subsequent definition of the strain of the strut. The parameters obtained, i.e. the maximum stress and strain, are used to define the masonry material with zero tensile strength simulated by the *Concrete01* constitutive model (Fig. 2(b)), [34]. The stress f_m is equal to 3.10 MPa and all infills have a thickness of 0.15 m. Additionally, a residual stress equal to 10% of the maximum stress is considered for numerical stability, which is reached at an interstorey drift five times the interstorey drift at maximum strength.

Geometric nonlinearities are incorporated in the form of P-Δ effects. Furthermore, soil structure interaction phenomena are not modelled and the building is considered fixed at the ground level. The first and the second fundamental periods of vibration of the buildings, with and without the masonry infills, are presented in Table 1. Finally, the average of the first two periods of the infilled structures and the first two periods of the bare structures T^* is determined (also shown in Table 1) to be used for the ground motion record selection. It is noted that involving the period of vibration of the bare structure when defining T^* is conceptually similar to accounting for the period elongation of the structure after yielding and failure of the infills, after which the behaviour of the structure will tend to that of the bare structure.

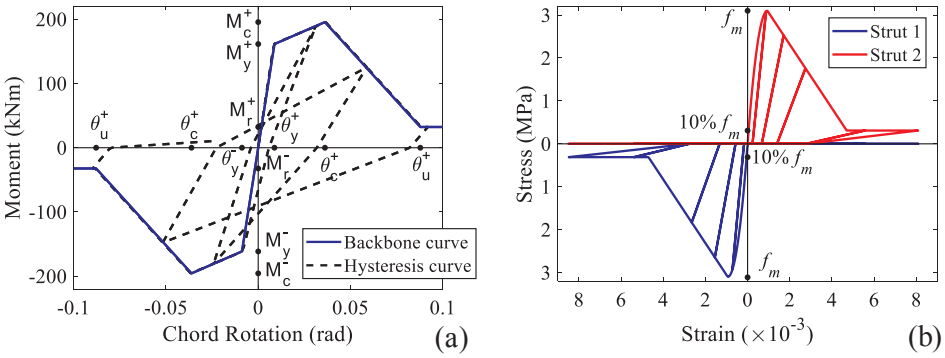

Fig. 2. Moment-rotation backbone curve and hysteresis loop simulation for a column (a) and stress – strain relationship of the diagonal struts (in compression), measured in the diagonal direction (b).

Table 1
First and second mode periods of vibration of the buildings.

Period\Building	3-storey	4-storey	5-storey
$[T_1, T_2]_{\text{infilled}}$	[0.31 s, 0.25 s]	[0.41 s, 0.31 s]	[0.52 s, 0.39 s]
$[T_1, T_2]_{\text{bare}}$	[0.73 s, 0.72 s]	[0.96 s, 0.93 s]	[1.18 s, 1.15 s]
T^*	0.5 s	0.66 s	0.82 s

4.2. Ground motion selection and analysis

The ground motion record selection is performed using the recently developed SelEQ software [24] using a Conditional Spectrum (CS) in terms of the 5% damped spectral acceleration (Sa) [35] as the target spectrum. After identifying the sources contributing to the hazard at the site (Lisbon), the probabilistic seismic hazard analysis of the site was performed within the SelEQ software using the open source software OpenQuake [36] and the seismic hazard model developed by the SHARE project [37]. The annual seismic hazard curve H_{IM} was determined at T^* for each building at the benchmark site and is shown in Fig. 3(a). For each source and four probabilities of exceedance, i.e. 30%, 10%, 5% and 2% in 50 years, the disaggregation of the hazard was performed at T^* and the contribution of each magnitude-distance (M-R) bins for the hazard was then computed. For each probability of exceedance, the results were aggregated and the contribution of each M-R pair and ground motion prediction equation to the exceedance of the spectral acceleration of interest was computed to determine a CS that considers the contributions of all individual M-R pairs using the methodology proposed in [38,39]. A preliminary record selection was performed using the NGA-WEST2 database [40] based on seismological and strong motion criteria. These criteria are: magnitude larger than 5.5, closest distance from source to site larger than 10 km, soil shear wave velocity, in upper 30 m of soil, greater than 200 m/s, a limit of five records from a single seismic event, a lowest useable frequency lower than 0.5 Hz, faulting scenarios compatible with the site (Lisbon), only free-field and far-field records. Subsequently, the final selection and scaling of a group of 40 bi-directional records (for each probability of exceedance) was carried out by ensuring compatibility between the target spectrum, i.e. the CS, and the average of the spectral accelerations of the 40 records, where the spectral acceleration of each record is defined by the geometric mean of the spectral accelerations of the two horizontal components of the record. SelEq ensures this compatibility by minimizing the difference between statistics of the target spectrum (i.e. the mean and standard deviation of the logarithms of the spectral accelerations) and the same statistics of the group, within a period range of 0.2 T^* and 1.5 T^*, as described in [24]. An additional criterion was included in the process which involves minimizing also the skewness of the logarithms of the spectral accelerations to a value close to zero for the same period range. This criterion is based on the fact that the spectral accelerations are expected to follow a multivariate lognormal distribution [41] and, therefore, the logarithms of the spectral accelerations are expected to follow a multivariate normal distribution. The scale factors (SF) of individual records that were involved during this record selection process range from 0.263 to 3.995. To illustrate the results of the ground motion selection process, Fig. 3(b) shows the geometric means of the selected 40 records along with the CS for the 30% in 50 years probability of exceedance for the 3-storey building. All the 40 records of a group defined for a certain probability of exceedance were then scaled using the SF shown in Table 2 to define *IM* levels whose spectral accelerations Sa(T^*) are also shown. Each group of records is only scaled to match a few *IM* levels in order to have the four

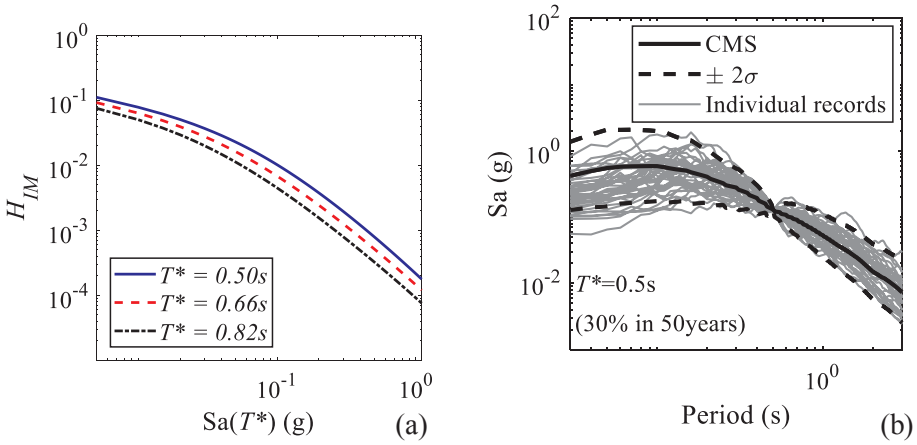

Fig. 3. The seismic hazard curves for the three buildings (a) and the CS with the geometric mean spectra of the 40 records for the 30% in 50 years probability of exceedance for the 3-storey building (b).

Table 2
Scale factors and corresponding spectral accelerations used in the MSA procedure.

Probability of exceedance	(*IM*)	Scale factor	Sa(T^* = 0.50 s) (g)	Scale factor	Sa(T^* = 0.66 s) (g)	Scale factor	Sa(T^* = 0.82 s) (g)
	(1)	0.38	0.05	0.41	0.04	0.40	0.03
	(2)	0.77	0.10	0.72	0.07	0.67	0.05
30% in 50 years	(3)	1.00	0.13	1.00	0.10	1.00	0.07
	(4)	1.54	0.20	1.45	0.14	1.48	0.11
	(5)	0.86	0.25	0.82	0.18	0.82	0.14
10% in 50 years	(6)	1.00	0.29	1.00	0.22	1.00	0.17
	(7)	1.21	0.35	1.19	0.26	1.23	0.21
	(8)	0.91	0.40	0.89	0.30	0.90	0.24
5% in 50 years	(9)	1.00	0.44	1.00	0.34	1.00	0.27
	(10)	1.20	0.53	1.22	0.41	1.21	0.32
	(11)	1.36	0.60	1.39	0.47	1.39	0.37
	(12)	0.92	0.67	0.91	0.52	0.91	0.42
2% in 50 years	(13)	1.00	0.73	1.00	0.57	1.00	0.46
	(14)	1.08	0.79	1.10	0.63	1.09	0.50
	(15)	1.16	0.85	1.20	0.69	1.17	0.54
	(16)	1.30	0.95	1.39	0.80	1.37	0.63
	(17)	1.44	1.05	1.57	0.90	1.54	0.71
	(18)	1.58	1.15	1.71	0.98	1.70	0.78
	(19)	1.71	1.25	1.83	1.05	1.83	0.84
	(20)	1.85	1.35	1.97	1.13	1.96	0.90

groups of records spanning a total of 20 *IM* levels. Values of SF equal to 1 correspond to the initial selection of a given group of 40 records that match the corresponding CS. The overall maximum and minimum SFs that are applied to any individual record, combining the scaling needed during the record selection process and the scaling to match the selected *IM* levels, are 7.8445 and 0.1078.

MSA was then performed following a procedure similar to the one proposed in [42] using the four sets of 40 records scaled according to Table 2 spanning the 20 *IM* levels. For the *regrouping* procedure, each group of 40 records is then regrouped into groups of 10, 20 and 30 records implementing selection criteria consistent with the criteria used for the initial selection to ensure compatibility between the new groups of 10, 20 and 30 records and the original group of 40 records. The *regrouping* procedure starts by defining the total number of combinations of m items (in this case 40) taken k (in this case, 10, 20 or 30) at a time, which is given by the binomial coefficient:

$$\binom{m}{k} = \frac{m!}{(m-k)!k!} \tag{6}$$

For example, for the group of 20 records, the binomial coefficient is equal to 1.3×10^{11}. However, not all combinations are valid since admissible groups of records need to represent a seismic scenario consistent with that of the reference group of size 40. Consistency is assumed to be verified when a ground motion group of size k meets three conditions consistent with the criteria that were used for the initial selection as described previously. These conditions are applied between statistics of the spectral values of each new group and the target spectrum, where the target spectrum now corresponds to the spectrum of the 40 records. As for the selection of the initial group of 40 records, the selected statistics are the mean, the standard deviation and the skewness of the logarithms of the spectral accelerations. Regarding the first two statistics, a variation of 10% is allowed between the statistics of the reference group of size 40 and the statistics of the new group with a lower size. With respect to the skewness, admissibility is checked by ensuring the skewness of the new group with a lower size cannot be rejected according to the standard error test for skewness [43], considering a significance level of 5% and the reference skewness of the group of size 40. Following this procedure, a total of 100 groups were created for each of the new group sizes (10, 20 and 30). These 100 groups can then be used to analyse the uncertainty associated with group-to-group variability.

5. Comparing the performance of the procedures for assessing the variability of fragility and failure rate estimates

5.1. Variability of the estimates of the fragility parameters

5.1.1. Deterministic limit state scenario

The MSA yielded 20 stripes of ISD_{max} and, to determine the ratios defined by Eq. (2), failure is considered to occur when ISD_{max} is higher than a limit value ISD_{cap} or when there is numerical failure of the model due to nonconvergence. For the deterministic limit state scenario, ISD_{cap} is set to 2.5%. One hundred fragility curves are constructed according to the *regrouping* procedure for the three buildings using all 20 stripes of demand. Fig. 4 shows the 100 fragility functions of the 3-storey building determined for the 100 groups of 20 records obtained by the *regrouping* procedure when all 20 stripes of demands are considered. One group of 20 records, termed parent group *i*, with parameters $\{\hat{\theta}, \hat{\beta}\}$ shown in Table 3, is randomly selected from the 100 groups to carry out the *bootstrap* procedure. Two *bootstrap* sample sizes of 100 and 500 are considered to analyse the sensitivity of the *bootstrap* estimates and the corresponding results are identified by the number in parentheses in Table 3. The fragility functions corresponding to the *bootstrap i (100)* case are shown in Fig. 4(a) along with the fragility function of the parent group *i*, which is represented by the thick black line. To emphasize some key points of the two procedures, Fig. 4(b) shows results similar to those of Fig. 4(a) but considering a different parent group *j*. As can be seen, the domain covered by the *bootstrap* fragility functions is not always the same and depends on the parent group. Statistics of the parameters of the fragility functions, i.e. their mean μ and variability values, the latter in terms of the standard deviation σ and of the coefficient of variation *CV*, are presented in Table 3 for all three buildings studied and for both procedures. Even though the discussion about the variability of the parameters is mostly focused on the values of σ, values of *CV* are also provided for all the results presented in this Section and in the following ones in order to better understand the magnitude of that variability.

By comparing the statistics obtained from *bootstrap (100)* and *bootstrap (500)* presented in Table 3, it appears that using a *bootstrap* sample size of 100 is adequate to estimate the selected statistics for all the considered case studies. The mean values, $\mu_{\hat{\theta}}$ and $\mu_{\hat{\beta}}$, are nearly identical and the differences in the σ are small (less than 15%). Therefore, subsequent results are only based on the *bootstrap (100)*

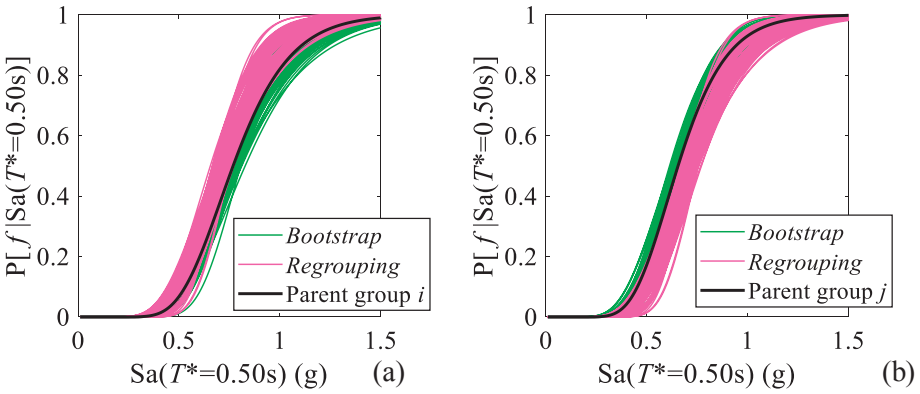

Fig. 4. Comparison of the 100 fragility functions of the 3-storey building obtained from the *regrouping* and the *bootstrap (100)* procedures using 20 stripes. Parent groups *i* and *j* are used for the *bootstrap* resampling in (a) and (b), respectively.

case. Furthermore, when comparing the performance of the *regrouping* and *bootstrap* procedures based on the visual analysis of Fig. 4 and on the statistics of Table 3, an overall good match can be observed between the corresponding statistics of the variability of the fragility function parameters, $\sigma_{\hat{\theta}}$ and $\sigma_{\hat{\beta}}$. It is noted, however, that the parent group that is selected for the *bootstrap* affects the fragility functions that are subsequently generated. With respect to the mean values of the parameters, which differ for the different parent groups, they can be either higher or lower than the corresponding parameters obtained with the *regrouping* procedure. Although this biased mean cannot be corrected since it only depends on the original data being bootstrapped, i.e. the parent group, it is not a relevant aspect of the procedure since bootstrapping is normally used to estimate the variability of the estimates and not their mean values. The variability values obtained by the *bootstrap* procedure, on the other hand, do not seem to vary substantially for the alternative parent groups, for both parameters examined. Furthermore, they are in good agreement with those obtained by the *regrouping* procedure for both parameters and for all case studies. Nevertheless, *bootstrap* seems to lead to marginally lower variability for most of the cases, in particular for parameter β.

To complement the previously presented results with cases involving different numbers of records, similar analyses were performed using groups of 30 and 10 records. Groups of 30 and 10 records are selected for being representative of larger and of smaller group sizes, respectively. Fragility function parameter statistics similar to those of Table 3 are presented in Tables 4 and 5, for the groups of size 30 and 10, respectively. As expected (e.g. see [19]), the results obtained for smaller groups of records using the *regrouping* and the *bootstrap* procedures exhibit a larger variability of both fragility estimates, while results obtained for the larger groups are the opposite. Despite the reduction in the variability of the estimates that is observed when using 30 records (Table 4), the trend of the results is similar to the one observed when using 20 records. As such, when using groups of 30 records, the variabilities obtained from the *regrouping* and from the *bootstrap* procedures are also very similar for both fragility parameters. On the other hand, using a small number of records, such as 10 (Table 5), can lead to large differences between the results of the two procedures. As can be seen from Table 5, these differences are present for both fragility parameters and their relative variations depend on the structure. It can thus be said that using an adequate number of records is crucial to ensure that *bootstrap* variability estimates can still be considered valid, despite the previously discussed inconsistency between the *regrouping* and the *bootstrap* procedures.

A further assessment of the performance of the two procedures is carried out by replicating this fragility curve analysis using a lower number of *IM* levels (i.e. fewer stripes). Although using a higher number of *IM* levels is generally suggested to reduce the fitting error, it is not uncommon to find situations where a much lower number of *IM* levels is used. Five *IM* levels covering uniformly the range of response of the structures are selected for the purpose of the present research. In particular, the lowest *IM* corresponds to the lowest *IM* value that contributes to the lower tail of the fragility curve of a given building, the highest *IM* corresponds to the maximum *IM* value considered for each building and contributes to the upper tail of the fragility curve. The remaining three *IM* levels are selected in order to cover the range of the fragility curves. Hence, referring to Table 2, stripes [7,11,15,18,20] are selected for the 3-storey building, stripes [8,11,15,18,20] are selected for the 4-storey building and stripes [8,14,16,18,20] are selected for the

Table 3
Statistics of the fragility function parameters due to group-to-group variability for the three buildings using 20 records and 20 stripes.

Building	Procedure	$\hat{\theta}$	$\mu_{\hat{\theta}}$	$\sigma_{\hat{\theta}}$	$CV_{\hat{\theta}}$(%)	$\hat{\beta}$	$\mu_{\hat{\beta}}$	$\sigma_{\hat{\beta}}$	$CV_{\hat{\beta}}$(%)
3-Storey	*Regrouping*	–	**0.72**	**0.026**	**3.58**	–	**0.28**	**0.040**	**14.38**
	Bootstrap i (100)	0.77	0.77	0.023	2.99	0.29	0.29	0.031	10.86
	Bootstrap i (500)	0.77	0.77	0.022	2.82	0.29	0.28	0.028	9.88
	Bootstrap j (100)	0.66	0.66	0.019	2.93	0.29	0.28	0.029	10.23
	Bootstrap j (500)	0.66	0.66	0.020	3.00	0.29	0.28	0.027	9.57
4-Storey	*Regrouping*	–	**0.59**	**0.020**	**3.39**	–	**0.26**	**0.034**	**13.04**
	Bootstrap i (100)	0.58	0.58	0.015	2.58	0.26	0.25	0.028	11.01
	Bootstrap i (500)	0.58	0.58	0.017	2.84	0.26	0.25	0.030	11.81
	Bootstrap j (100)	0.61	0.62	0.018	2.95	0.28	0.27	0.026	9.49
	Bootstrap j (500)	0.61	0.62	0.018	2.99	0.28	0.27	0.027	9.76
5-storey	*Regrouping*	–	**0.47**	**0.015**	**3.12**	–	**0.22**	**0.020**	**9.31**
	Bootstrap i (100)	0.47	0.47	0.014	2.89	0.24	0.23	0.027	11.77
	Bootstrap i (500)	0.47	0.47	0.012	2.55	0.24	0.23	0.026	11.14
	Bootstrap j (100)	0.49	0.49	0.012	2.50	0.22	0.22	0.026	11.87
	Bootstrap j (500)	0.49	0.49	0.012	2.54	0.22	0.22	0.023	10.66

Table 4
Statistics of the fragility function parameters due to group-to-group variability for the three buildings using 30 records and 20 stripes.

Building	Procedure	$\hat{\theta}$	$\mu_{\hat{\theta}}$	$\sigma_{\hat{\theta}}$	$CV_{\hat{\theta}}$(%)	$\hat{\beta}$	$\mu_{\hat{\beta}}$	$\sigma_{\hat{\beta}}$	$CV_{\hat{\beta}}$(%)
3-Storey	*Regrouping*	–	**0.71**	**0.016**	**2.22**	–	**0.28**	**0.022**	**7.95**
	Bootstrap i (100)	0.71	0.71	0.016	2.18	0.28	0.28	0.023	8.07
4-Storey	*Regrouping*	–	**0.59**	**0.012**	**2.04**	–	**0.27**	**0.020**	**7.28**
	Bootstrap i (100)	0.57	0.57	0.014	2.42	0.24	0.24	0.025	10.34
5-storey	*Regrouping*	–	**0.47**	**0.008**	**1.78**	–	**0.22**	**0.018**	**7.91**
	Bootstrap i (100)	0.47	0.47	0.009	1.88	0.22	0.21	0.018	8.37

5-storey building and new fragility curves are constructed using both the *regrouping* and the *bootstrap* procedures. The fragility curves developed for the three buildings using 20 records are presented in Fig. 5, while the respective statistics of the fragility parameter estimates are shown in Table 6. Given the good agreement of the results obtained using 100 and 500 *bootstrap* samples for this case as well, only the results obtained for the *bootstrap* sample size of 100 are presented and discussed.

The reduction of the number of stripes appears to have little effect on the mean estimates of the parameters for both the *regrouping* and the *bootstrap* procedures, as shown by the good agreement of the mean values of Table 3 and Table 6. Nevertheless, such as for the observations derived for 20 stripes, the mean values of $\hat{\theta}$ and $\hat{\beta}$ obtained for the *bootstrap* procedure depend on the selection of the parent group. With respect to the variability of the parameter estimates, Unlike the previous case, using only 5 stripes leads to a much higher variability of the parameter estimates. This effect can be initially attributed to the higher epistemic error that is unavoidably introduced by having a lower number of points to fit the fragility function (i.e. fewer stripes). However, this increase of the variability doesn't affect equally the two procedures, i.e. the *regrouping* and the *bootstrap*. While the standard deviation σ of both $\hat{\theta}$ and $\hat{\beta}$ is marginally higher for the *regrouping* procedure (they increase by 20%, on average), almost all values of σ increase to more than twice their initial value for the *bootstrap* procedure. These results show that the inconsistency between the *regrouping* samples and the *bootstrap* pseudo-samples (see Section 3.1) has a larger impact in the variability of the fragility parameter estimates when a lower number of stripes is considered. As such, when focusing on the comparative assessment of the *regrouping* and the *bootstrap* procedure for the case where only 5 stripes are used, the *regrouping* procedure is seen to lead systematically to a lower variation of the parameters. This effect is graphically illustrated in Fig. 5 and can be quantitatively observed in Table 6. It can be seen that the standard deviation of both $\hat{\theta}$ and $\hat{\beta}$ is larger for the *bootstrap* procedure, leading to an overestimation of $\sigma_{\hat{\beta}}$ up to 50% and of $\sigma_{\hat{\theta}}$ up to 35%.

Conclusions similar to those obtained for the groups of 20 records can also be seen for the case involving groups of 30 records, as shown in Table 7. Although the variability of the parameter estimates is inherently lower when compared to that of the 20 records and 5 stripes, using 30 records and 5 stripes with the *regrouping* procedure yields insignificant differences in the *CV* of both parameters when compared to the case involving 30 records and 20 stripes. On the contrary, a similar comparison for the results obtained for the *bootstrap* procedure shows that the *CV* of both parameters more than doubles when using only 5 stripes. When using groups of 10 records and 5 stripes (results shown in Table 8), on the other hand, larger differences are found in the variability of the parameters with respect to the case involving 20 stripes. For the *regrouping* procedure variations can be up to 80%, but much larger values are found for the results obtained from the *bootstrap* procedure where variations can go up to 300%. In the overall, it can be concluded that the *bootstrap* procedure can provide adequate estimates of the variability of parameters, i.e. comparable with those obtained from the *regrouping* procedure, as long as an adequate number of records and number of stripes are employed. If these conditions are not met, the variability estimates obtained from *bootstrap* can either under- or overestimate the true variability of the parameters.

5.1.2. Probabilistic limit state scenario

The evolution of the fragility function parameter estimates is examined next when the effect of the uncertainty of the capacity model is also taken into account according to Eq. (5), where m_{Cap} is equal to the deterministic capacity of 2.5% and ε_{Cap} is a lognormal random variable with unit median and β_{ε} equal to 0.5. Although only the lognormal model is adopted in the present research to express the uncertainty related to the capacity model error [26], similar results are expected for different statistical models. Monte Carlo (MC) analysis is performed using a sample of 10 capacity values [22] that are generated using stratified sampling [44] and the fragility functions are determined using the *regrouping* and the *bootstrap* (parent group *i* considering 100 *bootstrap* samples) procedures. The fragility functions obtained for the 3-storey building are presented in Fig. 6, along with the corresponding fragility functions that do not account for uncertainty in capacity for comparison purposes. The parameter estimate statistics for all buildings are presented in Tables 9 and 10, corresponding to the results obtained from groups of 20 records when 20 and 5 stripes are considered, respectively.

As expected, introducing variability in the limit state capacity results in larger $\hat{\beta}$ values for all fragility curves, representing the record-to-record variability and the uncertain capacity. This effect can be observed in Fig. 6 by the lower steepness of all the new fragility functions and in Tables 9 and 10 by the larger $\mu_{\hat{\beta}}$ values, when compared to those of Tables 3 and 6, respectively. Depending on the building, the increase of $\mu_{\hat{\beta}}$ can be from 50% to more than 100% and occurs in a similar way in the results of both the *regrouping* and the *bootstrap* procedures. The

Table 5
Statistics of the fragility function parameters due to group-to-group variability for the three buildings using 10 records and 20 stripes.

Building	Procedure	$\hat{\theta}$	$\mu_{\hat{\theta}}$	$\sigma_{\hat{\theta}}$	$CV_{\hat{\theta}}$(%)	$\hat{\beta}$	$\mu_{\hat{\beta}}$	$\sigma_{\hat{\beta}}$	$CV_{\hat{\beta}}$(%)
3-Storey	*Regrouping*	–	**0.70**	**0.048**	**6.78**	–	**0.27**	**0.070**	**25.59**
	Bootstrap i (100)	0.74	0.74	0.031	4.23	0.27	0.27	0.032	11.72
4-Storey	*Regrouping*	–	**0.59**	**0.036**	**6.13**	–	**0.25**	**0.063**	**24.72**
	Bootstrap i (100)	0.55	0.55	0.018	3.31	0.17	0.16	0.030	18.83
5-storey	*Regrouping*	–	**0.46**	**0.024**	**5.25**	–	**0.22**	**0.031**	**13.97**
	Bootstrap i (100)	0.53	0.53	0.019	3.66	0.24	0.24	0.038	16.07

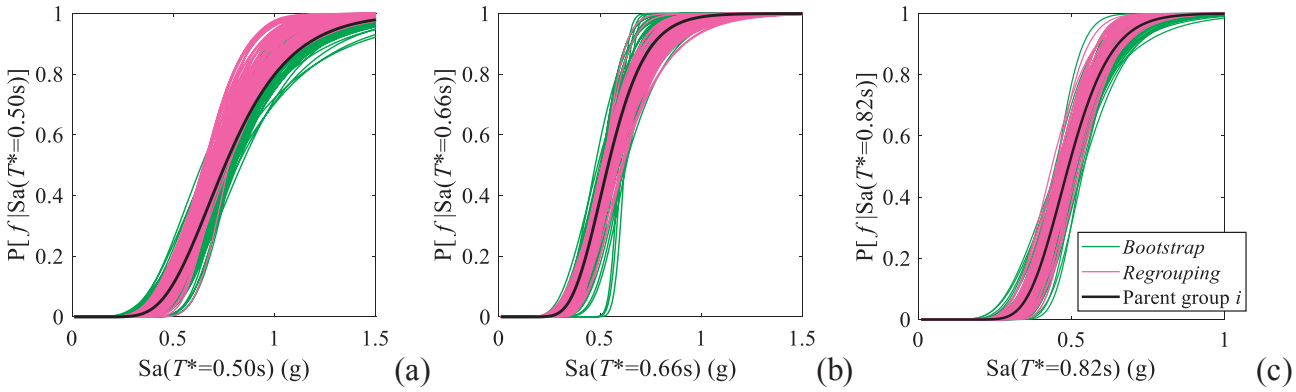

Fig. 5. Comparison of the 100 fragility functions of the 3-storey (a), 4-storey (b) and 5-storey (c) buildings obtained from the *bootstrap* and the *regrouping* procedures using 20 records and 5 stripes.

Table 6
Statistics of the fragility function parameters due to group-to-group variability for the three buildings using 20 records 5 stripes.

Building	Procedure	$\hat{\theta}$	$\mu_{\hat{\theta}}$	$\sigma_{\hat{\theta}}$	$CV_{\hat{\theta}}$(%)	$\hat{\beta}$	$\mu_{\hat{\beta}}$	$\sigma_{\hat{\beta}}$	$CV_{\hat{\beta}}$(%)
3-Storey	*Regrouping*	–	**0.71**	**0.029**	**4.02**	–	**0.29**	**0.047**	**16.06**
	Bootstrap i (100)	0.76	0.74	0.039	5.18	0.34	0.31	0.060	19.37
4-Storey	*Regrouping*	–	**0.56**	**0.022**	**4.01**	–	**0.28**	**0.038**	**13.58**
	Bootstrap i (100)	0.54	0.55	0.030	5.53	0.27	0.25	0.057	23.11
5-storey	*Regrouping*	–	**0.49**	**0.018**	**3.72**	–	**0.20**	**0.031**	**15.12**
	Bootstrap i (100)	0.49	0.49	0.020	4.07	0.22	0.21	0.043	20.41

variability in capacity, on the other hand, has a much smaller effect on $\mu_{\hat{\theta}}$, which remains almost unchanged for both procedures and for all three buildings analysed.

Regarding the comparison of the statistics of the parameter estimates when 20 or 5 stripes of intensities are used, the observations are similar to those of Section 5.1.1, i.e. to the case involving a deterministic limit state. As such, when a larger number of stripes is used (Table 9), the *regrouping* and *bootstrap* procedures provide similar results both in terms of mean values and in terms of variability, although the *regrouping* procedure generally yields a larger variability. When a smaller number of stripes is used (Table 10), the mean values of the estimates predicted by both procedures are similar, but the variability estimates obtained by *bootstrap* can be as large as twice the values obtained when using 20 stripes. Regarding the variability of the parameters obtained with the *regrouping* procedure, the increase that is observed is much smaller. As seen in the results presented in the previous Section, the inconsistency issue between the *regrouping* samples and the *bootstrap* pseudo-samples has a much larger effect when a lower number of stripes is used.

Fig. 6 highlights an additional feature of the results obtained by introducing the uncertainty in capacity: a reduction of the variability of both $\hat{\theta}$ and $\hat{\beta}$ with respect to the case where this uncertainty is not considered. This effect can be seen for both procedures by the thinner range of variation of the new fragility functions in Fig. 6 and, quantitatively, by the smaller standard deviation values of $\hat{\theta}$ and $\hat{\beta}$ in Tables 9 and 10 when compared to those of Tables 3 and 6, respectively. Even though this result appears to be counterintuitive, it is a direct outcome of the selected procedure to develop the fragility functions according to the EDP-based approach when uncertainty in capacity is involved using the MC approach.

Results obtained for the group sizes of 30 and 10 are presented in Tables 11–14 for both cases in terms of number of stripes. The trends regarding the reduced variability observed for the groups of size 20 when the uncertain capacity limit state is used instead of the deterministic capacity limit state, are also found for these two other group sizes. As such, variability estimates of Tables 11 and 13 are lower when compared to those of Tables 4 and 5, respectively, and variability estimates of Tables 12 and 14 are also lower when compared to those of Tables 7 and 8, respectively. Furthermore, differences between the results obtained for a given group size using 20 and 5 *IMs* are smaller when capacity uncertainty is involved. As such, when the *regrouping* procedure is employed, groups of 10 records using 5 stripes can also be seen to lead to low variability estimates when compared to the case involving 20 stripes (Tables 13 and 14). The *bootstrap* procedure, on the other hand, leads to a larger variability of the fragility parameters when fewer stripes are used, rendering it incompatible with *regrouping* regardless of the number of records that is used. Ultimately, the conclusions found for the analyses involving a deterministic capacity limit

Table 7
Statistics of the fragility function parameters due to group-to-group variability for the three buildings using 30 records and 5 stripes.

Building	Procedure	$\hat{\theta}$	$\mu_{\hat{\theta}}$	$\sigma_{\hat{\theta}}$	$CV_{\hat{\theta}}$(%)	$\hat{\beta}$	$\mu_{\hat{\beta}}$	$\sigma_{\hat{\beta}}$	$CV_{\hat{\beta}}$(%)
3-Storey	*Regrouping*	–	**0.71**	**0.019**	**2.69**	–	**0.29**	**0.027**	**9.34**
	Bootstrap i (100)	0.70	0.70	0.031	4.36	0.30	0.29	0.048	16.51
4-Storey	*Regrouping*	–	**0.56**	**0.013**	**2.36**	–	**0.29**	**0.021**	**7.39**
	Bootstrap i (100)	0.54	0.54	0.024	4.46	0.27	0.26	0.043	16.42
5-storey	*Regrouping*	–	**0.49**	**0.012**	**2.51**	–	**0.21**	**0.018**	**8.87**
	Bootstrap i (100)	0.48	0.48	0.018	3.81	0.22	0.21	0.042	19.78

Table 8
Statistics of the fragility function parameters due to group-to-group variability for the three buildings using 10 records and 5 stripes.

Building	Procedure	$\hat{\theta}$	$\mu_{\hat{\theta}}$	$\sigma_{\hat{\theta}}$	$CV_{\hat{\theta}}$(%)	$\hat{\beta}$	$\mu_{\hat{\beta}}$	$\sigma_{\hat{\beta}}$	$CV_{\hat{\beta}}$(%)
3-Storey	*Regrouping*	–	**0.70**	**0.058**	**8.32**	–	**0.27**	**0.093**	**34.09**
	Bootstrap i (100)	0.76	0.77	0.051	6.65	0.29	0.28	0.070	25.07
4-Storey	*Regrouping*	–	**0.56**	**0.049**	**8.74**	–	**0.26**	**0.089**	**34.55**
	Bootstrap i (100)	0.51	0.53	0.062	11.79	0.17	0.11	0.078	72.30
5-storey	*Regrouping*	–	**0.48**	**0.032**	**6.70**	–	**0.19**	**0.046**	**24.04**
	Bootstrap i (100)	0.57	0.56	0.026	4.71	0.17	0.16	0.063	40.56

state can be seen to be applicable to analyses that consider uncertainty in the capacity limit state. Nonetheless, differences between the results obtained with the *regrouping* and the *bootstrap* procedures are much smaller in the former analyses. In the following Section, additional findings are presented to further analyse the effects of propagating these results when computing the failure rate.

5.2. Variability of the estimate of the failure rate

5.2.1. Deterministic limit state scenario

Failure rates are determined from Eq. (3) using the fragility functions obtained in Section 5.1.1 and the seismic hazard curves that were presented in Section 4.2. The statistics of the $\hat{\lambda}_f$ values obtained for the sets of fragility functions determined in Section 5.1.1 are presented in Tables 15 and 16 for the cases involving groups of 20 records and 20 and 5 stripes, respectively. It is noted that the first column of values in Tables 15 and 16 corresponds to the values of $\hat{\lambda}_f$ obtained with the fragility function of the parent group *i*.

Results indicate that computing $\hat{\lambda}_f$ for the fragility functions derived from the *regrouping* or the *bootstrap* procedure yields similar mean values of $\hat{\lambda}_f$, irrespective of the number of stripes. The variability of $\hat{\lambda}_f$ expressed by $\sigma_{\hat{\lambda}_f}$, however, can be marginally larger when using the *regrouping*-based fragility functions and 20 stripes. On the contrary, when only 5 stripes are used, the value of $\sigma_{\hat{\lambda}_f}$ for the *bootstrap* procedure can be up to 50% larger than the value obtained for the *regrouping* procedure. Therefore, although the relationship between the fragility curves and the failure rates is inherently nonlinear (accounting also for the shape of the seismic hazard curve), the variability of the fragility function parameters propagates to the variability of the failure rate. It is also noted that variability values obtained from fragility curves involving 5 stripes and the *bootstrap* procedure are systematically larger than the corresponding values derived from fragility curves involving 20 stripes and, in some cases, they exhibit an increase of more than 100%. Therefore, the issues related with the inconsistency between the *regrouping* samples and the *bootstrap* pseudo-samples that are highlighted in the results of the previous sections propagate in a similar way to the failure rate estimates. Results obtained considering different sizes of group records follow similar trends and are omitted herein for the sake of brevity.

5.2.2. Probabilistic limit state scenario

The failure rates presented in this Section are determined from Eq. (3) using the seismic hazard curve presented in Section 4.2 and the fragility functions obtained in Section 5.1.2, which involve record-to-record variability and uncertainty of the limit state capacity. The statistics of $\hat{\lambda}_f$ are shown in Tables 17 and 18 for the cases involving groups of 20 records and for 20 and 5 stripes, respectively. The results indicate that including the variability of the capacity leads to higher mean values of $\hat{\lambda}_f$ but to a lower variability of $\hat{\lambda}_f$. The reduction in the variability of $\hat{\lambda}_f$ reflects the reduction in the variability of the fragility function parameters discussed in Section 5.1.2. This observation is valid for the results obtained by the *bootstrap* or the *regrouping* procedures and is consistent for all buildings considered. Finally, as for the results in the previous Section, when using a lower number stripes, the variability of $\hat{\lambda}_f$ obtained from the *regrouping* procedure is seen to increase between 10% and 30%, while that obtained by the *bootstrap* procedure is much larger, increasing between 60% and 100%. The effects of the inconsistency between the *regrouping* samples and the *bootstrap* pseudo-samples are therefore similar to those found in the results of the previous Section, further supporting the proposed conditions for using the *bootstrap* procedure.

6. Conclusions

The uncertainty in estimating the probabilistic seismic performance of structures associated to the use of a certain finite-size group of ground motion records, i.e. the group-to-group variability, was examined for several situations. The *regrouping* and the *bootstrap* procedures were applied to quantify this variability, even though the validity of the latter was disputed due to its incompatibility with cases where the probabilistic seismic performance assessment enforces specific criteria for the ground motion selection. Although *bootstrap* is widely

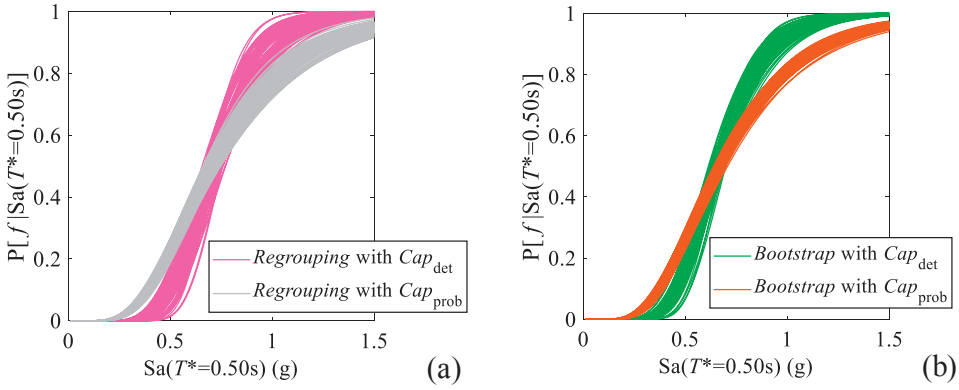

Fig. 6. Fragility functions of the 3-storey building obtained by the *regrouping* (a) and by the *bootstrap* (b) procedure with deterministic and probabilistic capacity using 20 stripes.

Table 9
Statistics of the fragility function parameters due to group-to-group variability for the three buildings and probabilistic capacity using 20 records and 20 stripes.

Building	Procedure	$\hat{\theta}$	$\mu_{\hat{\theta}}$	$\sigma_{\hat{\theta}}$	$CV_{\hat{\theta}}$(%)	$\hat{\beta}$	$\mu_{\hat{\beta}}$	$\sigma_{\hat{\beta}}$	$CV_{\hat{\beta}}$(%)
3-Storey	*Regrouping*	–	**0.71**	**0.020**	**2.86**	–	**0.47**	**0.025**	**5.40**
	Bootstrap i (100)	0.75	0.75	0.015	2.05	0.48	0.48	0.019	3.99
4-Storey	*Regrouping*	–	**0.58**	**0.016**	**2.77**	–	**0.46**	**0.025**	**5.37**
	Bootstrap i (100)	0.55	0.56	0.008	1.46	0.41	0.41	0.017	4.21
5-storey	*Regrouping*	–	**0.47**	**0.013**	**2.87**	–	**0.52**	**0.021**	**4.07**
	Bootstrap i (100)	0.46	0.46	0.008	1.78	0.52	0.52	0.017	3.21

Table 10
Statistics of the fragility function parameters due to group-to-group variability for the three buildings and probabilistic capacity using 20 records and 5 stripes.

Building	Procedure	$\hat{\theta}$	$\mu_{\hat{\theta}}$	$\sigma_{\hat{\theta}}$	$CV_{\hat{\theta}}$(%)	$\hat{\beta}$	$\mu_{\hat{\beta}}$	$\sigma_{\hat{\beta}}$	$CV_{\hat{\beta}}$(%)
3-Storey	*Regrouping*	–	**0.71**	**0.021**	**2.90**	–	**0.47**	**0.030**	**6.36**
	Bootstrap i (100)	0.74	0.75	0.028	3.69	0.49	0.49	0.039	8.06
4-Storey	*Regrouping*	–	**0.57**	**0.017**	**2.98**	–	**0.47**	**0.029**	**6.21**
	Bootstrap i (100)	0.55	0.55	0.015	2.68	0.41	0.41	0.031	7.49
5-storey	*Regrouping*	–	**0.47**	**0.015**	**3.28**	–	**0.54**	**0.023**	**4.27**
	Bootstrap i (100)	0.45	0.45	0.012	2.68	0.54	0.55	0.035	6.47

Table 11
Statistics of the fragility function parameters due to group-to-group variability for the three buildings and probabilistic capacity using 30 records and 20 stripes.

Building	Procedure	$\hat{\theta}$	$\mu_{\hat{\theta}}$	$\sigma_{\hat{\theta}}$	$CV_{\hat{\theta}}$(%)	$\hat{\beta}$	$\mu_{\hat{\beta}}$	$\sigma_{\hat{\beta}}$	$CV_{\hat{\beta}}$(%)
3-Storey	*Regrouping*	–	**0.70**	**0.012**	**1.69**	–	**0.46**	**0.016**	**3.46**
	Bootstrap i (100)	0.69	0.69	0.010	1.51	0.45	0.45	0.015	3.28
4-Storey	*Regrouping*	–	**0.58**	**0.010**	**1.65**	–	**0.47**	**0.016**	**3.47**
	Bootstrap i (100)	0.56	0.56	0.008	1.47	0.45	0.45	0.014	3.03
5-storey	*Regrouping*	–	**0.47**	**0.008**	**1.63**	–	**0.52**	**0.014**	**2.78**
	Bootstrap i (100)	0.47	0.47	0.006	1.21	0.50	0.50	0.014	2.89

Table 12
Statistics of the fragility function parameters due to group-to-group variability for the three buildings and probabilistic capacity using 30 records and 5 stripes.

Building	Procedure	$\hat{\theta}$	$\mu_{\hat{\theta}}$	$\sigma_{\hat{\theta}}$	$CV_{\hat{\theta}}$(%)	$\hat{\beta}$	$\mu_{\hat{\beta}}$	$\sigma_{\hat{\beta}}$	$CV_{\hat{\beta}}$(%)
3-Storey	*Regrouping*	–	**0.70**	**0.013**	**1.79**	–	**0.46**	**0.018**	**3.98**
	Bootstrap i (100)	0.69	0.69	0.019	2.81	0.46	0.46	0.030	6.49
4-Storey	*Regrouping*	–	**0.58**	**0.010**	**1.76**	–	**0.48**	**0.019**	**3.92**
	Bootstrap i (100)	0.56	0.56	0.014	2.47	0.47	0.47	0.029	6.23
5-storey	*Regrouping*	–	**0.46**	**0.009**	**2.02**	–	**0.54**	**0.016**	**2.96**
	Bootstrap i (100)	0.46	0.46	0.009	1.93	0.53	0.53	0.027	5.06

Table 13
Statistics of the fragility function parameters due to group-to-group variability for the three buildings and probabilistic capacity using 10 records and 20 stripes.

Building	Procedure	$\hat{\theta}$	$\mu_{\hat{\theta}}$	$\sigma_{\hat{\theta}}$	$CV_{\hat{\theta}}$(%)	$\hat{\beta}$	$\mu_{\hat{\beta}}$	$\sigma_{\hat{\beta}}$	$CV_{\hat{\beta}}$(%)
3-Storey	*Regrouping*	–	**0.69**	**0.036**	**5.20**	–	**0.46**	**0.051**	**11.01**
	Bootstrap i (100)	0.71	0.70	0.020	2.88	0.47	0.47	0.023	4.94
4-Storey	*Regrouping*	–	**0.58**	**0.028**	**4.82**	–	**0.47**	**0.045**	**9.68**
	Bootstrap i (100)	0.56	0.56	0.013	2.32	0.46	0.46	0.021	4.57
5-storey	*Regrouping*	–	**0.47**	**0.026**	**5.50**	–	**0.52**	**0.044**	**8.50**
	Bootstrap i (100)	0.53	0.53	0.013	2.41	0.60	0.60	0.029	4.92

applied for determining uncertainty estimates, the randomness condition of the *bootstrap* pseudo-samples is not compatible with the situation of selecting several group of records compatible with a certain seismic scenario. The *regrouping* procedure proposed in this study, on the other hand, does not have this incompatibility since it considers additional constrains accounting for the required spectral matching conditions for each new ground motion group sample. Due to the higher computational cost of the latter though, the performance of the two procedures in determining the variability of fragility function parameter estimates and seismic risk estimates was analysed in order to establish the conditions under which the *bootstrap* procedure is expected to lead to small errors.

Table 14
Statistics of the fragility function parameters due to group-to-group variability for the three buildings and probabilistic capacity using 10 records and 5 stripes.

Building	Procedure	$\hat{\theta}$	$\mu_{\hat{\theta}}$	$\sigma_{\hat{\theta}}$	$CV_{\hat{\theta}}$(%)	$\hat{\beta}$	$\mu_{\hat{\beta}}$	$\sigma_{\hat{\beta}}$	$CV_{\hat{\beta}}$(%)
3-Storey	*Regrouping*	–	**0.69**	**0.038**	**5.46**	–	**0.46**	**0.057**	**12.48**
	Bootstrap i (100)	0.70	0.71	0.035	5.02	0.46	0.46	0.047	10.23
4-Storey	*Regrouping*	–	**0.58**	**0.031**	**5.45**	–	**0.48**	**0.056**	**11.69**
	Bootstrap i (100)	0.56	0.57	0.023	4.03	0.48	0.47	0.044	9.24
5-storey	*Regrouping*	–	**0.46**	**0.029**	**6.33**	–	**0.54**	**0.046**	**8.45**
	Bootstrap i (100)	0.54	0.54	0.018	3.41	0.58	0.58	0.043	7.45

Table 15
Statistics of $\hat{\lambda}_f$ due to group-to-group variability for the three buildings using 20 records and 20 stripes.

Building	Procedure	$\hat{\lambda}_f(\times 10^{-4})$	$\mu_{\hat{\lambda}_f}(\times 10^{-4})$	$\sigma_{\hat{\lambda}_f}(\times 10^{-5})$	$CV_{\hat{\lambda}_f}$(%)
3-Storey	*Regrouping*	–	**4.46**	**3.54**	**7.94**
	Bootstrap i (100)	3.88	5.30	3.70	6.98
4-Storey	*Regrouping*	–	**4.12**	**2.31**	**5.61**
	Bootstrap i (100)	4.18	4.16	2.23	5.36
5-storey	*Regrouping*	–	**3.82**	**2.26**	**5.92**
	Bootstrap i (100)	3.81	3.82	2.29	5.98

Table 16
Statistics of $\hat{\lambda}_f$ due to group-to-group variability for the three buildings using 20 records and 5 stripes.

Building	Procedure	$\hat{\lambda}_f(\times 10^{-4})$	$\mu_{\hat{\lambda}_f}(\times 10^{-4})$	$\sigma_{\hat{\lambda}_f}(\times 10^{-5})$	$CV_{\hat{\lambda}_f}$(%)
3-Storey	*Regrouping*	–	**4.57**	**3.94**	**8.61**
	Bootstrap i (100)	4.23	4.19	6.02	14.35
4-Storey	*Regrouping*	–	**4.68**	**3.46**	**7.40**
	Bootstrap i (100)	4.87	4.73	5.27	11.13
5-storey	*Regrouping*	–	**3.55**	**2.75**	**7.73**
	Bootstrap i (100)	3.53	3.49	3.19	9.13

Table 17
Statistics of $\hat{\lambda}_f$ due to group-to-group variability and probabilistic capacity for the three buildings using 20 stripes.

Building	Procedure	$\hat{\lambda}_f(\times 10^{-4})$	$\mu_{\hat{\lambda}_f}(\times 10^{-4})$	$\sigma_{\hat{\lambda}_f}(\times 10^{-5})$	$CV_{\hat{\lambda}_f}$(%)
3-Storey	*Regrouping*	–	**5.75**	**2.66**	**4.62**
	Bootstrap i (100)	5.26	6.30	2.83	4.49
4-Storey	*Regrouping*	–	**5.34**	**1.87**	**3.49**
	Bootstrap i (100)	5.35	5.35	1.68	3.14
5-storey	*Regrouping*	–	**5.29**	**2.12**	**4.01**
	Bootstrap i (100)	5.45	5.45	1.87	3.43

Table 18
Statistics of $\hat{\lambda}_f$ due to group-to-group variability and probabilistic capacity for the three buildings using 5 stripes.

Building	Procedure	$\hat{\lambda}_f(\times 10^{-4})$	$\mu_{\hat{\lambda}_f}(\times 10^{-4})$	$\sigma_{\hat{\lambda}_f}(\times 10^{-5})$	$CV_{\hat{\lambda}_f}$(%)
3-Storey	*Regrouping*	–	**5.68**	**3.24**	**5.70**
	Bootstrap i (100)	5.36	5.37	4.72	8.79
4-Storey	*Regrouping*	–	**5.46**	**2.12**	**3.88**
	Bootstrap i (100)	5.45	5.44	2.65	4.87
5-storey	*Regrouping*	–	**5.49**	**2.77**	**5.06**
	Bootstrap i (100)	5.78	5.77	3.64	6.31

The findings show that the *regrouping* and the *bootstrap* procedures provide comparable results for both variables examined (i.e. the fragility function parameters and the failure rates) when a relatively high number of stripes was used to define the probabilistic demand model (i.e. 20 *IMs*) combined with an adequate number of records (i.e. more than 10). When using a lower number of stripes, i.e. 5, the variability of the parameter estimates determined from the *regrouping* procedure did not change substantially from the case involving 20 *IMs*, thus showing the robustness of the procedure. On the other hand, the variability quantified using the *bootstrap* procedure was systematically much larger than in the case involving 20 *IMs*. In some cases, the variability estimates of the examined parameters more than doubled.

The variability of the fragility function parameters was further examined when additional uncertainty was involved by introducing a probabilistic capacity model. In this case, the results showed a reduction of the variability of all parameters, contradicting the potential expectation that an increase in the variability of the input would result in an increase in the variability of the output. This reduction in variability was consistently observed in the results obtained from the *regrouping* and the *bootstrap* procedures, for all group sizes, and also for the two scenarios involving a different number of stripes. Still, when using a low number of stripes, the *bootstrap* procedure led to a significant increase of the variability estimates, while those obtained from the *regrouping* procedure showed much smaller differences with respect to the case involving 20 stripes. This variability further propagated to the failure rate estimates, leading to results with similar trends.

In the overall, although the *regrouping* procedure requires additional computational effort, it provides robust variability estimates for the fragility function parameters and the failure rates, independently of the number of stripes that is used, as long as an adequate number of records is used. On the contrary, the variability estimates obtained from the *bootstrap* procedure are highly dependent on the number of selected stripes. *Bootstrap* results were considered to be adequate when obtained using 20 stripes as well as a group of at least 20 records. In addition, the relative performance of both procedures was not seen to be affected by the selected capacity modelling approach. Nevertheless, more analyses are required in order to validate these findings for cases including additional sources uncertainties, such as modelling uncertainties. Finally, all conclusions obtained are site-specific, and their validity for different sites characterized by different seismic hazard therefore requires further verification.

Acknowledgements

Financial support of the Portuguese Foundation for Science and Technology, through the PhD grant of the first author (PD/BD/113681/2015)PD/BD/113681/2015, is gratefully acknowledged. Authors also acknowledge the financial support of Project POCI-01- 0145-FEDER-007457 - CONSTRUCT - Institute of R&D In Structures and Construction funded by FEDER funds through COMPETE2020 - Programa Operacional Competitividade e Internacionalização (POCI) - and by national funds through FCT - Fundação para a Ciência e a Tecnologia.

References

[1] FEMA P-58. Seismic performance assessment of buildings. vol. III. Washington,

D.C.: Federal Emergency Management Agency; 2012.
[2] Abrahamson NA, Bommer JJ. Probability and uncertainty in seismic hazard analysis. Earthquake spectra 2005;21(2):603–7.
[3] Haselton CB, Baker JW, Bozorgnia Y, Goulet CA, Kalkan E, Luco N, et al. Evaluation of ground motion selection and modification methods: Predicting median interstory drift response of buildings. PEER 2009 (Technical Report 2009/01); 2009.
[4] fib Seismic assessment and retrofit of reinforced concrete buildings. Bulletin n°24, Fédération Internationale du Béton. Lausanne, Switzerland; 2003.
[5] Gokkaya BU, Baker JW, Deierlein GG. Quantifying the impacts of modeling uncertainties on the seismic drift demands and collapse risk of buildings with implications on seismic design checks. Earthquake Eng Struct Dyn 2016;45(10):1661–83.
[6] Jalayer F, Iervolino I, Manfredi G. Structural modeling uncertainties and their influence on seismic assessment of existing RC structures. Struct Saf 2010;32(3):220–8.
[7] Vamvatsikos D, Fragiadakis M. Incremental dynamic analysis for estimating seismic performance sensitivity and uncertainty. Earthquake Eng Struct Dyn 2010;39(2):141–63.
[8] Celarec D, Dolšek M. The impact of modelling uncertainties on the seismic performance assessment of reinforced concrete frame buildings. Eng Struct 2013;52:340–54.
[9] Miano A, Jalayer F, Prota A. Considering structural modeling uncertainties using Bayesian cloud analysis. Proceedings of the 6th ECCOMAS thematic conference on computational methods in structural dynamics and earthquake engineering (COMPDYN 2017) Rhodes, Greece, 15-17 June 2017. 2017.
[10] Gardoni P, Der Kiureghian A, Mosalam KM. Probabilistic capacity models and fragility estimates for reinforced concrete columns based on experimental observations. J Eng Mech 2002;128(10):1024–38.
[11] Liel AB, Haselton CB, Deierlein GG, Baker JW. Incorporating modeling uncertainties in the assessment of seismic collapse risk of buildings. Struct Saf 2009;31(2):197–211.
[12] Iervolino I. Assessing uncertainty in estimation of seismic response for PBEE. Earthquake Eng Struct Dyn 2017;46(10):1711–23.
[13] Bradley BA, Lee DS. Accuracy of approximate methods of uncertainty propagation in seismic loss estimation. Struct Saf 2010;32(1):13–24.
[14] Baker JW, Cornell CA. Uncertainty propagation in probabilistic seismic loss estimation. Struct Saf 2008;30(3):236–52.
[15] Bradley BA. Epistemic uncertainties in component fragility functions. Earthquake Spectra 2010;26(1):41–62.
[16] Tothong P, Luco N. Probabilistic seismic demand analysis using advanced ground motion intensity measures. Earthquake Eng Struct Dyn 2007;36(13):1837–60.
[17] Rajeev P, Franchin P, Pinto PE. Increased accuracy of vector-IM-based seismic risk assessment? J Earthquake Eng 2008;12(S1):111–24.
[18] Silva V, Crowley H, Pinho R, Varum H. Extending displacement-based earthquake loss assessment (DBELA) for the computation of fragility curves. Eng Struct 2013;56:343–56.
[19] Eads L, Miranda E, Krawinkler H, Lignos DG. An efficient method for estimating the collapse risk of structures in seismic regions. Earthquake Eng Struct Dyn 2013;42(1):25–41.
[20] Efron B, Tibshirani R. An introduction to the bootstrap. CRC Press; 1994.
[21] Baker JW. Efficient analytical fragility function fitting using dynamic structural analysis. Earthquake Spectra 2015;31(1):579–99.
[22] Bakalis K, Vamvatsikos D. Seismic fragility functions via nonlinear response history analysis. J Struct Eng 2018;144(10):04018181.
[23] Jalayer F, Cornell CA. Alternative non-linear demand estimation methods for probability-based seismic assessments. Earthquake Eng Struct Dyn 2009;38(8):951–72.
[24] Macedo L, Castro JM. SelEQ: an advanced ground motion record selection and scaling framework. Adv Eng Softw 2017;114:32–47.
[25] Lupoi G, Franchin P, Lupoi A, Pinto PE. Seismic fragility analysis of structural systems. J Eng Mech 2006;132(4):385–95.
[26] Cornell CA, Jalayer F, Hamburger RO, Foutch DA. Probabilistic basis for 2000 SAC federal emergency management agency steel moment frame guidelines. J Struct Eng 2002;128(4):526–33.
[27] McKenna F, Fenves GL. Opensees 2.5.0. Computer Software. UC Berkeley, Berkeley (CA); 2011. http://opensees.berkeley.edu.
[28] Panagiotakos TB, Fardis MN. Deformations of reinforced concrete members at yielding and ultimate. Struct J 2001;98(2):135–48.
[29] Haselton CB, Goulet CA, Mitrani-Reiser J, Beck JL, Deierlein GG, Porter KA, et al. An assessment to benchmark the seismic performance of a code-conforming reinforced-concrete moment-frame building. Pacific Earthquake Engineering Research Center (PEER 2007/1); 2008.
[30] Dolšek M, Fajfar P. Post-test analyses of the SPEAR test building. University of Ljubljana; 2005. http://www.ikpir.com/projects/spear.
[31] Zareian F, Medina RA. A practical method for proper modeling of structural damping in inelastic plane structural systems. Comput Struct 2010;88(1–2):45–53.
[32] Žarnić R, Gostič S. Masonry infilled frames as an effective structural sub-assemblage. In: Fajfar Krawinkler, editor. Seismic design methodologies for the next generation of codes. Balkema: Rotterdam; 1997. p. 335–46.
[33] Dolšek M, Fajfar P. The effect of masonry infills on the seismic response of a four-storey reinforced concrete frame-a deterministic assessment. Eng Struct 2008;30(7):1991–2001.
[34] Noh NM, Liberatore L, Mollaioli F, Tesfamariam S. Modelling of masonry infilled RC frames subjected to cyclic loads: state of the art review and modelling with OpenSees. Eng Struct 2017;150:599–621.
[35] Baker JW. Conditional mean spectrum: tool for ground-motion selection. J Struct Eng 2010;137(3):322–31.
[36] Pagani M, Monelli D, Weatherill G, Danciu L, Crowley H, Silva V, et al. OpenQuake engine: an open hazard (and risk) software for the global earthquake model. Seismol Res Lett 2014;85(3):692–702.
[37] Woessner J, Laurentiu D, Giardini D, Crowley H, Cotton F, Grünthal G, et al. The 2013 European seismic hazard model: key components and results. Bull Earthq Eng 2015;13(12):3553–96.
[38] Lin T, Haselton CB, Baker JW. Conditional spectrum-based ground motion selection. Part I: hazard consistency for risk-based assessments. Earthquake Eng Struct Dyn 2013;42(12):1847–65.
[39] Lin T, Haselton CB, Baker JW. Conditional spectrum-based ground motion selection. Part II: intensity-based assessments and evaluation of alternative target spectra. Earthquake Eng Struct Dyn 2013;42:1867–84.
[40] Ancheta TD, Darragh RB, Stewart JP, Seyhan E, Silva WJ, Chiou BSJ, et al. NGA-West2 database. Earthquake Spectra 2014;30(3):989–1005.
[41] Jayaram N, Baker JW. Statistical tests of the joint distribution of spectral acceleration values. Bull Seismol Soc Am 2008;98(5):2231–43.
[42] Christovasilis IP, Cimellaro GP, Barani S, Foti S. On the selection and scaling of ground motions for fragility analysis of structures. In: Proceedings of 2nd European conference on earthquake engineering and seismology, Istanbul, Turkey; 2014.
[43] Tabachnick BG, Fidell LS. Using multivariate statistics. 3rd ed. New York: Harper Collins; 1996.
[44] Iman RL, Conover WJ. A distribution-free approach to inducing rank correlation among input variables. Commun Stat Simul Comput 1982;11(3):311–34.